SAND2018-9497C

AIMFAST for Heliostats: Canting Tool for Long Focal Lengths

Charles E. Andraka

Sandia National Laboratories
PO 5800, MS 1127
Albuquerque NM 87185-1127
ceandra@sandia.gov

Abstract. Accurate canting, or alignment, of heliostat facets is critical to the optical success of CSP tower systems. Canting accuracy for large fields must typically be on the order of 0.25mrad RMS. To date, heliostats are canted through dimensional control such as fixtures or touch probes, with potentially much higher error.

AIMFAST (Alignment Implementation for Manufacturing using Fringe Analysis Slope Technique) is a fringe reflection (deflectometry) tool utilized to provide rapid, accurate optically-based canting of mirror facets on multi-facet CSP systems. AIMFAST was originally developed in support of 40-facet dish deployments by Stirling Energy systems in 2009 [1] and generalized to arbitrary dish systems in 2013 [2]. AIMFAST was demonstrated to meet alignment goals of <0.25 mrad RMS on dish systems, and accounts for structural deflections caused by gravity as the tracking structure rotates.

This paper presents the extension of AIMFAST to large area heliostats. Multi-facet heliostats provide challenges to the fringe reflection method due to the nearly flat optical structure, leading to either multiple cameras or very large projection screens instead of LCD flat panels. Key elements include characterization of target image distortion from multiple projectors, boresighting of the subject heliostat, automated detection of errors, and automated adjustment tool interface.

BACKGROUND

Large scale 100MW$_e$ class tower plants have heliostats up to 1.6km slant range from the receiver. The DOE Sunshot assessment of current optical performance assumes a total reflected beam error of 3.39mrad RMS, or 1.2mrad RMS surface slope error in each axis [3]. This corresponds to a canting accuracy (surface angle) of 0.25 mrad RMS in each axis. To date, deployed heliostats in medium-to-large installations have been canted with mandrels or touch probes, which are positional canting tools rather than optical canting tools. Touch probes typically contact the front surface of rear-silvered glass. Typical near-commercial and deployed heliostat facets measured at Sandia with SOFAST have facet slope errors on the order of 1.5mrad RMS in each axis (unpublished data, some more recent facets are better than 1mrad RMS). By positionally measuring a very limited number of points on the facet, the canting accuracy is limited to the surface slope accuracy, or 1.5 mrad.

A baseline plant was modelled in NREL's System Advisor Model (SAM) [4], utilizing a surround field, a nominal 100mW$_e$ rating with storage, producing approximately 400GWh$_e$ per year. The modelled system results in an LCOE of 10.41 US Cents/kWh$_e$. and had a total beam optical error of 3.39 mrad RMS [1]. The canting error was increased from 0.25mrad RMS to 1.5mrad RMS, while holding the receiver size constant. The LCOE increases to 10.94, primarily due to increased spillage. In a second case, the structure deflections were increased from 0.25mrad RMS to 1.0mrad RMS in addition to the canting error increase, resulting in an LCOE of 11.22. Table 1 shows the cases considered, and the impact to annual costs in generating the 400GWh$_e$ each year.

This highly simplified analysis indicates that there is significant cost to poor canting, and that current canting tools may fall significantly short of design expectations. Early optical methods that view static reflected targets principally

provide lines of information optically, which is an improvement over positional point information, but still limits canting accuracy to about 0.7 mrad RMS based on dish alignment trials [5-7]

Fringe reflection or deflectometry has been introduced for full-surface detailed characterization of mirror systems [8-11]. In this method, a camera views a reflection of an active target in the subject mirror system. A series of sinusoidal fringe patterns are presented on the active target, and straightforward mathematical analysis can determine the surface normal vector at each point [9]. We previously utilized this data in a multi-facet system to implement automated canting of dish systems [1, 5]. AIMFAST was developed for production line alignment of dish systems, and utilized internal data for much of the system setup, avoiding the need for total station surveying. In addition, AIMFAST was shown to accurately incorporate Finite Element Analysis (FEA) predictions of structural deflections to optimize the alignment at a different tracking elevation than the alignment elevation angle. AIMFAST was successfully implemented at the Stirling Energy Systems Maricopa 60-dish facility, and demonstrated alignment accuracies of 0.1 mrad RMS [5]. On a dish system, the camera and target are placed near the 2-f location, limiting the size of the needed active target area. However, on heliostat systems with near-flat mirrors, the 2-f distance is long and inaccessible, so the target must be roughly twice the size of the mirror system, or multiple cameras must be utilized [8].

In this paper we present the extensions and modifications to AIMFAST to accommodate 100m² class heliostats in a production environment. These modifications are developed and tested on a laboratory-scale surrogate heliostat.

Table 1. Financial impact of canting error.

Case	Slope Error (mrad)	Canting (mrad)	Structure (mrad)	Total Reflected Beam Error	LCOE (real)
Nominal	1.2	0.25	0.25	3.39	10.41
Increase canting error	1.9	1.5	0.25	5.39	10.94
Increase canting and structural error	2.14	1.5	1.00	6.04	11.22

MODIFICATIONS

Large Target

In order to accommodate the large area (~100m²) heliostat, either the projector screen would need to be 21m x 21m with a single camera, or 11m x 11m with up to 5 cameras. Due to schedule limitations, and the need for space around the heliostat to work, we pursued a large area projection screen with multiple projectors and single camera. In production, the target screen would be on the ceiling of the facility, approximately 10m above the heliostat. High intensity (7000 lumen) laser-light projectors were identified for the production case. In development, we utilized existing 2-3k lumen projectors in a subscale laboratory arrangement.

A key element of calibration is to characterize the distortion of the target screen pixel layout due to the projector lens, keystoning, and other installation errors. In AIMFAST, this is accomplished by projecting a grid, and then analyzing the images taken with a calibrated camera to determine the actual grid dimensions. The grid line intersections are located, and points in between are interpolated locally. We implemented a similar scheme in the new version. However, we needed to account for the potential discontinuity between the projections from the pair of projectors. A single Windows figure was extended across both projectors, and the grid pattern line closest to the transition between projectors was doubled, with a line on each projector. Thus, existing interpolation schemes could be utilized on the continuous grid within each projector image, and since there is a gridline at the edge of each projection, there is no data between these two gridlines, and no interpolation needed. This effectively accounts for the discontinuity.

Images of the projected grid are taken from several angles, and photogrammetry performed to locate each grid point. This requires calibration of the camera lens. However, this resulted in unsatisfactory reprojections of the points from each camera location, indicative of limited lens calibration accuracy. Instead, we allowed the camera lens distortion parameters to also be optimized during the photogrammetry, in addition to the gridpoint locations. This resulted in acceptable accuracy, and eliminates the need to calibrate the wide-angle camera lens.

The screen distortion calculation requires a known length in each direction in the camera field of view in images of the grid pattern. In the lab, we manually measured the vertical and horizontal centerlines of the grid. However, this

may prove impractical at full scale, on the ceiling, and can change if the projector setup changes. Therefore we propose to implement fixed LED's in at least 3 locations on the screen during assembly, which can be used as known location fiducials. Alternatively, the edges of the physical screen could be utilized.

Boresighting

AIMFAST for dishes utilized reflective fiducials at the engine location on the boom to provide substantially out-of-plane references, which aided in accurate photogrammetry to determine the dish pose relative to the camera. The lack of out-of-plane references on the heliostat requires alternate means of pose refinement. An interim solution used in development reflects the screen center (crosshairs) from the center of the heliostat, to the center of the camera, resulting in a determinate pose of the heliostat. This approach assumes the mirrors, on average, are reasonably aligned initially, which may not be an accurate assumption. In production, the target screen will be installed horizontally above the heliostat, and the heliostat frame can be checked for horizontal with bubble levels, providing a known pose in two rotational angles. Alternatively, laser distance measurements from the four corner mirrors to the center of the target screen can be used to determine the relative pose, rather than relying on the target being horizontal.

Automated Tool Interface

A simple TCPIP protocol is developed to communicate with adjustment tools or teams. The tool, preferably an automated adjustment tool, requests data for the current mirror facet. AIMFAST then characterizes the pose of that facet relative to the design pose (canting), and provides adjustment details back to the tool. The adjustment for each screw is provided, along with the total canting error in mrad/100. This protocol can provide the information to a Heads Up Display (HUD) for manual adjustment, or an automated wrench for automatic adjustment. The new protocol allows the tooling system to request any number of facets' angles simultaneously, allowing multiple tools. The protocol utilizes standard TCPIP libraries and ASCII messages to simplify implementation in user tools.

Error Trapping

A key element of AIMFAST is interleaving of image display and image acquisition, resulting in data collection at up to 7.5 frames per second. However, sometimes overhead in Windows or MatLab can result in timing mistakes, which results in bad data. This occurs when an image is only partly displayed when the camera triggers a frame, or possibly the frame is triggered before the image even begins to display. The result is wrong positional data for the facet reflected target points. This error had been detected visually in positional data plots in the past, and the data run is simply repeated. However, with the integration of automated tools, the system must automatically trap such errors and re-test. Otherwise, the facet will move to the wrong position, and move back again on the next iteration.

The Fringe Reflection method includes a temporal drill-down, with increasingly fine fringe patterns to refine the surface normal for each viewed pixel. For error trapping, we compare the determined position at each level of drill-down to that determined on the prior level, for every pixel on the mirror system. Through experimentation, a deviation threshold, and a percentage of points exceeding this deviation threshold, was developed to accurately capture errors.

Subscale Heliostat Prototype

The projection screen during initial development was 3.5m x 8.5m. A subscale 4-facet heliostat with approximately 4m² area was utilized in initial code development. Two-projector testing was performed on a 3.5m square target area with the camera on one edge. AIMFAST in production will utilize a ceiling-mounted projection screen with a horizontal heliostat, allowing easy access to adjustment screws. A single camera will be utilized through a small hole in the center of the screen.

The initial 4-facet heliostat worked for basic development. However, the adjustments were coarse, sticky, and non-repeatable. In addition, the frame was flexible. Finally, prospective AIMFAST users desired to verify operation on a representative heliostat with 24 facets. Therefore, we developed a second laboratory-scale heliostat, also 4m² in area, but with 24 facets, Fig. 1. A more robust support frame was utilized. In order to verify repeatability, the adjustment screws were designed to provide the same angular tilt for each screw turn as the full-scale heliostat. This resulted in a thread pitch of 100 threads per inch (0.25mm thread pitch). A system of spherical washers and spring washers ensures the adjustment does not impose significant moments into the mirror.

Figure 1. Single-facet test stand (left) and 24-facet lab-scale heliostat after initial alignment (right).

A single facet prototype was tested to ensure this adjustment scheme was repeatable. Automated tooling has not been developed, so manual adjustments with approximate screw turns were incorporated. After this system was debugged, it was implemented on a 24-facet prototype heliostat.

The projectors were mounted on stands on each side of the room, and a 3.5m square area illuminated. The projectors had to be separately adjusted to provide near-linear brightness response. Internal projector adjustments were used until both projectors provided similar response as determined by the AIMFAST radiometric calibration routine. Then the two projectors together were calibrated.

RESULTS

Large Target

The modified intersection routines placed a grid line on each side of the discontinuity between projectors, Fig. 2. It is imperative that the projections do not overlap, though a small gap is acceptable. The fringe patterns are continuous across the two projections by using a single Windows figure. Figure 3 shows that the intersections are successfully found on each side of the discontinuity. The revised code determines which gridline is closest to the discontinuity, places it at the discontinuity, doubles the line, and searches for an intersection from each horizontal direction.

Figure 4 shows the resulting distortion characterization for the dual-projector system. The darker (blue and green) vectors indicate positional deviation from the rectangular design grid, and shows key stoning on each projector. The flow of the distortion is smooth from point to point, representative of normal lens or angular errors. The position of each gridpoint is taken as the arithmetic mean of the position as seen by each photogrammetry camera position. In this case, three camera positions were utilized. The red vectors indicate the difference between the position projected by each camera image and the mean position. These vectors are amplified to exaggerate the error. The projection errors compared to the mean are all less than 2mm, compared to over 20mm when the camera lens was separately characterized. The standard deviation of positional differences is 0.34mm. The AIMFAST code interpolates (local cubic spline) for points between the gridpoints.

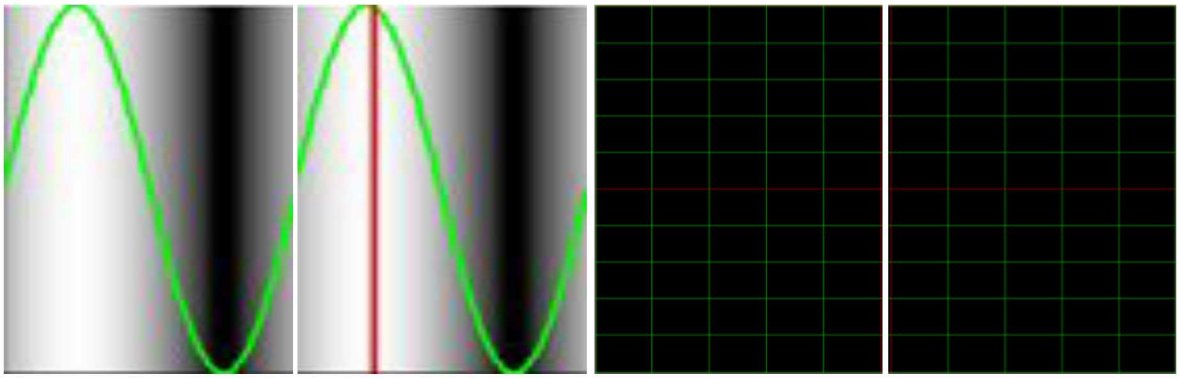

Figure 2. Two-projector target. Left, fringe patter extends across two projector images smoothly by using a single Windows figure. Right, the grid line in the characterization grid is doubled at the discontinuity, shown in red.

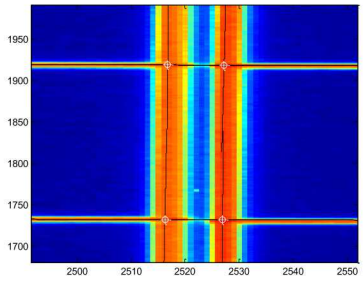

Figure 3. Line intersections along the projection discontinuity. Modified algorithms separated the lines into left and right components. The algorithm successfully acquires both sets of points.

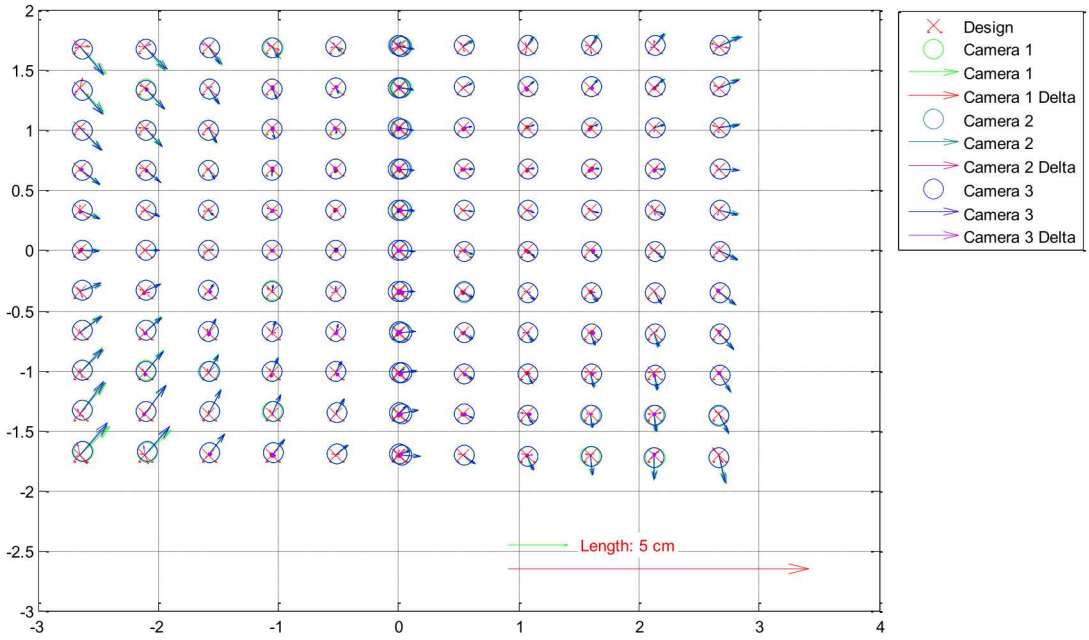

Figure 4. Distortion characterization of the combined screen. The distortions "flow" smoothly, characteristic of lens and keystone distortions. The green and blue vectors indicate distortion from different camera viewpoints. The red vectors indicate different apparent locations from different camera views.

Error Trapping

Figure 5 shows the horizontal normalized screen (target) position for each pixel as calculated by the deflectometry system. The left side shows artifacts due to improper timing (from SOFAST characterization of a single facet), while the right side shows smooth positional gradients typical of a good mirror with good timing (AIMFAST, 4-facet lab heliostat). Visual inspection would normally lead to re-testing the left mirror. Figure 6 shows this same data as a slice through the mirror system (a single vertical position), and shows the variation from each drill-down pass to the next. In the bad data case (left), later passes deviate significantly from earlier passes as the calculated position jumps from one fringe to another due to the errors in image acquisition. In the right image, the finer fringe patterns result in a refinement of the coarse pattern without major deviations.

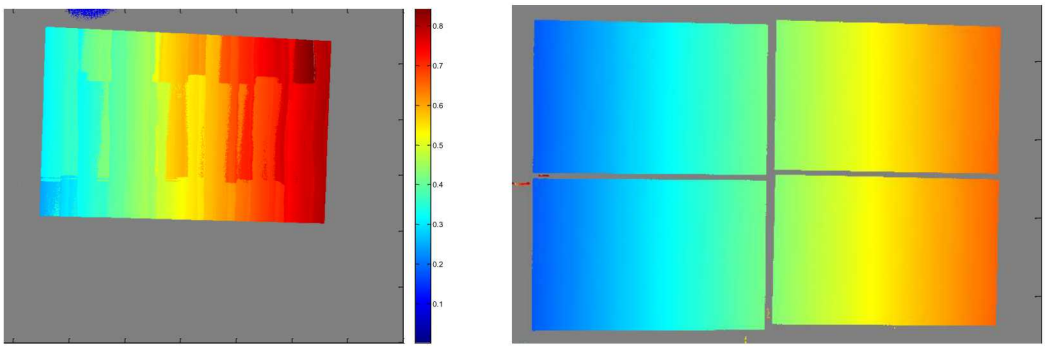

Figure 5. Plot of horizontal positional data. Left: Bad data on a single facet (from SOFAST). Right: Good data from the 4-facet laboratory heliostat.

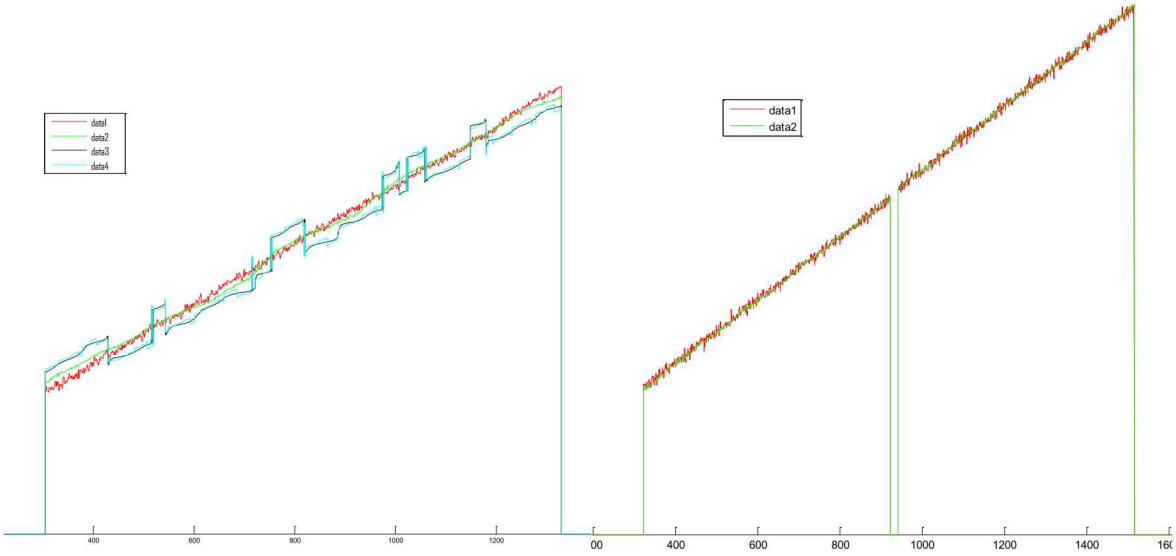

Figure 6. Slice of temporal drill-down data for good data (right, two levels of drill-down) and bad data (left, four levels of drill-down). The new code compares this data at all points, not just a slice through the data.

Through experimentation with a large number of datasets with and without error, we set the threshold deviation at 10% of the width of a single fringe in the current fringe pattern. If more than 5% of the data on the facet exceeded this level of change from the prior pass, then the data was declared bad. A typical good dataset had less than 0.5% of the points deviating greater than this threshold, while a typical bad dataset typically had greater than 50% of the points exceed this threshold, making this error check quite robust.

Subscale Heliostat Measurements

The single facet was initially aligned. Then ½ and 1 turn deviations were introduced on a single adjustment screw. After each adjustment, AIMFAST again scanned the mirror and reported required adjustment. The adjustments were applied manually, and so may contain some uncertainty. After each deviated position, the facet was restored to center by introducing the requested correction. Figure 7 shows the AIMFAST-reported results of these adjustments. Each deviated position was attained twice, and the center nominal position was attained 10 times. The aligned (center) points had a maximum error under 0.001” (0.025mm), with less than 0.12 mrad total angular error reported. Only 1 iteration was used to approach each position. This exercise shows that the fine adjustment screw system is capable of repeatable positioning, and suitable for implementation on the 24-facet array.

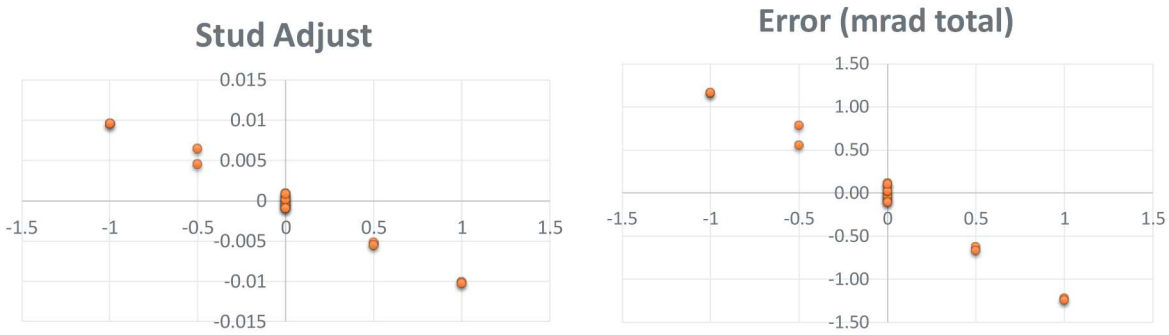

Figure 7. Single facet adjustment repeatability testing. The studs were repeatedly manually adjusted ½ or 1 turn, and then the position measured with AIMFAST. The left image shows the requested screw adjustment to return to nominal position, while the right shows the error in mrad. Each deviated location has two datapoints, while the center point has 10 points.

The 24-facet surrogate heliostat was fabricated using the same methods as the single-facet device. Figure 8 Left shows the initial alignment error with the facets visually leveled. Unfortunately, no data was collected prior to this visual alignment. Since some facets needed more than 20 turns adjustment, a motorized socket was used to initially position the facets based on AIMFAST input. Then two more iterations were applied using a manual socket, with turns as small as 10% of a turn of the screw, or 0.025mm. During this operation, we found that several of the screw assemblies were galled during fabrication, leading to non-repeatable inputs. These were repaired in place before final adjustments. One facet could not be repaired in time for publication, and is not considered in the final plot presented. Figure 8 Right shows the post-alignment canting errors. The facets are mounted with three studs: a pivot stud centered on one end, and two adjusting studs at the top and bottom about 1/3 of the facet length in from the opposite end. These stud locations are at the root of the vectors in Fig. 8. Each facet is approximately 0.61m x 0.25m.

Excluding facet 6 from the results, the RMS canting error indicated by AIMFAST is 0.092mrad RMS vertically, and 0.022mrad RMS horizontally. The vertical error is higher due to the shorter distance between screws, coupled with manual adjustment. Automated adjustment is likely to improve this result further.

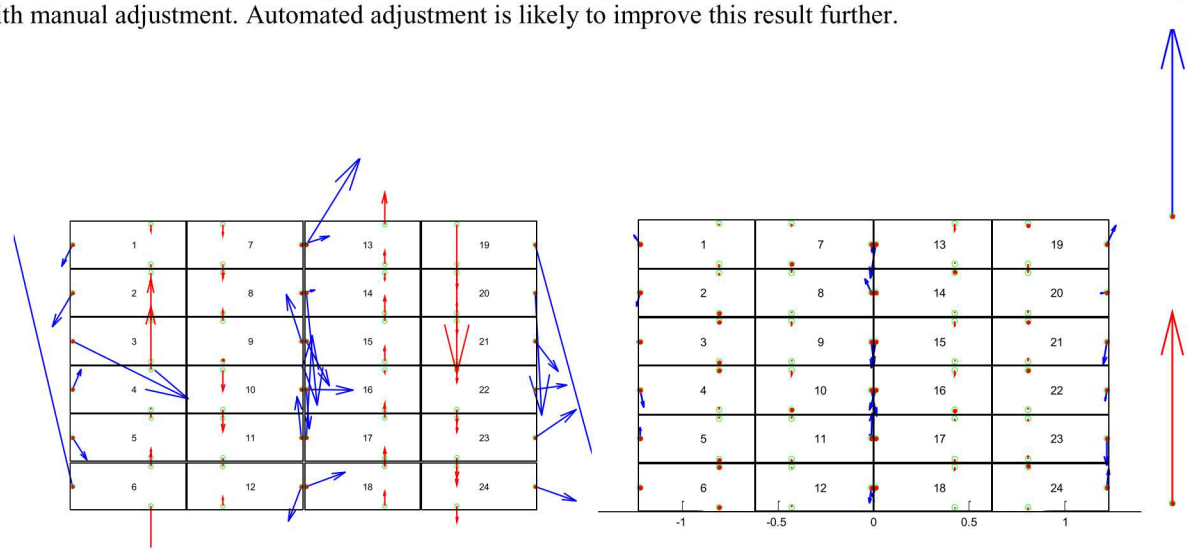

Figure 8. 24-Facet Lab Heliostat before and after final alignment. Facet 6 adjustment screws could not be adjusted due to severe galling. The blue vectors represent total canting error of each facet, while the red vectors indicate the adjustment needed at each screw. The red reference arrow is 1mm of adjustment, while the blue is 1 mrad of total canting error. Facet 6 is excluded from the right hand image.

NEXT STEPS

Initial results of AIMFAST adapted to heliostats are promising. The system successfully measures facet canting errors on multi-facet flat reflectors, and provides adjustments needed to match design canting.

After repairing or modifying additional adjustment screws, we will verify repeatability of alignment by randomly imposing adjustments, and then verifying that AIMFAST correctly discerns the amount of imposed adjustment, and that making the AIMFAST-suggested adjustment restores heliostat performance. We will verify the canting by on-sun verification of slant range after each iteration of repeatability testing, including at various slant ranges.

AIMFAST assumes the facets are rigid bodies with 3 mounts. The algorithms will be modified to accommodate over-constrained mirror facets with more than three adjustments, and will adjust the shape as well as the canting rotation.

Finally, AIMFAST's user interface will be substantially improved, removing development features and providing a clean interface to system operators. Likewise, a detailed user manual will be developed to ensure success by third-party users.

ACKNOWLEDGEMENTS

Sandia National Laboratories is a multimission laboratory managed and operated by National Technology & Engineering Solutions of Sandia, LLC, a wholly owned subsidiary of Honeywell International Inc., for the U.S. Department of Energy's National Nuclear Security Administration under contract DE-NA0003525.

I would like to acknowledge the support of SolarReserve in designing and manufacturing the surrogate heliostats utilized in development, as well as collaborating in the understanding of current method limitations and production line needs and requirements. I also acknowledge Roger Buck of Sandia, who provided valuable hands-on support in the implementation of the laboratory setup.

REFERENCES

[1] Andraka, C. E., Finch, Nolan, Yellowhair, Julius, Trapeznikov, Kirill, Carlson, Jeff, Myer, Brian, Stone, Brad, Hunt, Kirby, 2011, "AIMFAST: An Alignment Tool Based On Fringe Reflection Methods Applied To Dish Concentrators," Journal of Solar Energy Engineering, 133(031018-1).

[2] Andraka, C. E., 2013, "AIMFAST Generalization: A Rapid Alignment Characterization Tool for Arbitrary Dish Concentrators," SolarPACES 2013, Las Vegas, NV, Elsevier.

[3] Kolb, G. J., C.K. Ho, T.R. Mancini, J.A. Gary, 2011, "Power Tower Technology Roadmap and Cost Reduction Plan," Sandia National Laboratiores, Albuquerque, NM.

[4] Blair, N., DiOrio, N., Freeman, J., Gilman, P., Janzou, S., Neises, T., and Wagner, M., 2018, "System Advisor Model (SAM) General Description (Version 2017.9.5)," No. NREL/TP-6A20-70414, NREL, Golden, CO.

[5] Andraka, C. E., Yellowhair, Julius, Finch, Nolan, Carlson, Jeff, Francis, Matt, Hunt, Kirby, Raffa, Carl, Kulaga, Tom, "AIMFAST: Initial Dish System Alignments Results Using Fringe Reflection Methods," Proc. ASME 5th International Conference on Energy Sustainability.

[6] Andraka, C. E., Diver, R. B., and Rawlinson, K. S., 2003, "Improved alignment technique for dish concentrators," International Solar Energy Conference, Kohala Coast, HI, USA.

[7] Diver Jr, R. B., 1992, "Mirror Alignment Techniques for Point-Focus Solar Concentrators," No. SAND92-0668, Sandia National Laboratories, Albuquerque NM.

[8] Andraka, C. E., Finch, Nolan, Yellowhair, Julius, Francis, Matt, Hunt, Kirby, Kulaga, Tom, 2011, "SOFAST Facet Characterization for Heliostats: Extensions and Difficulties," Proc. SolarPACES.

[9] Andraka, C. E., Sadlon, Scott, Myer, Brian, Trapeznikov, Kirill, Liebner, Christina, 2013, "Rapid Reflective Facet Characterization Using Fringe Reflection Techniques," Journal of Solar Energy Engineering, 136(1), p. 11.

[10] Ulmer, S., März, T., Prahl, C., Reinalter, W., and Belhomme, B., 2011, "Automated high resolution measurement of heliostat slope errors," Solar Energy, 85(4), pp. 681-687.

[11] Marz, T., Prahl, C., Ulmer, S., Wilbert, S., and Weber, C., "Validation of Two Optical Measurement Methods for the Qualification of the Shape Accuracy of Mirror Panels for Concentrating Solar Systems," J. Sol. Energy Eng. Trans.-ASME, 133(3).